Electronic Supplementary Information (ESI)
For

Modulating Charge Transfer over Metal-organic Framework Nanocomposites for NIR light-boosted Photothermal Conversion

Liqian Liu, *Yite Li*, *Lei Wang**, Zhigang Xie*

L. Liu, Y. Li, L. Wang, Z. Xie

State Key Laboratory of Polymer Physics and Chemistry

Changchun Institute of Applied Chemistry

Chinese Academy of Sciences

Changchun, Jilin 130022, P. R. China

leiwang@ciac.ac.cn; xiez@ciac.ac.cn

L. Liu, Y. Li, Z. Xie

School of Applied Chemistry and Engineering

University of Science and Technology of China

Hefei 230026, P. R. China

Table of Contents

Section S1. Experimental section

S1.1 Chemicals. All chemical materials (2, 2-dichloroacetic acid, Zirconyl chloride octahydrate, Phosphomolybdic Acid Hydrate (TMA), Dithiothreitol (DTT), polylactic acid (PLA), Rhodamine B, Trichloromethane, ethanol) and N, N-dimethylformamide (DMF) used were purchased commercially without further purification. DCFH-DA ROS Detection Kit was purchased from Beyotime Biotechnology Co., Ltd. Live/Dead Cell Staining Kit and SYTO 9 were purchased from Nanjing KeyGen Biotech Co., Ltd. Bacteria Petri dishes were purchased from Guangzhou Jet Bio-Filtration Co., Ltd. The preparation of Meso-Tetra (4-carboxyphenyl) porphyrin (TCPP) refers to the method described in the literature [1].

S1.2 Analytical techniques. TEM images of as-prepared nanoparticles were determined by a JEOL JEM-1011 electron microscope with 100 kV as accelerating voltage. SEM images were acquired by an FEI/Philips XL-30 scanning electron microscope with an accelerating voltage of 5 kV. All UV−vis spectrometric measurements were analyzed by a Shimadzu UV-2450 spectrophotometer. The nanoparticle size distribution and zeta potential were performed using a Malvern Zeta-sizer Nano. The powder X-ray diffraction (PXRD) patterns were obtained with a Smartlab diffractometer using Cu Kα radiation (40 kV, 40 mA) with a scan range of 2theta from 2 to 45. The fluorescence emission spectra were monitored with the PerkinElmer LS-55 spectrofluorophotometer. Fluorescence lifetime was recorded on an Edinburgh FLS980 fluorescence spectrometer using the time-correlated single-

photon counting (TCSPC) method. The nitrogen adsorption isotherms were conducted on a Micromeritics ASAP 2010 analyzer. X-ray photoelectron spectroscopy (XPS) was measured by a Thermo Scientific ESCALAB 250 Multitechnique Surface Analysis. Inductively coupled plasma mass spectrometry (ICP-MS) analysis was performed on an Agilent 7700x series ICP-MS instrument. Thermogravimetric analysis (TGA) was carried out by using a TGA/DSC 1 (Mettler-Toledo, Switzerland), which scanned from 40 to 800 ℃ at a heating rate of 10 ℃ min^{-1} under air gas. FT-IR was recorded with a Bruker ALPHA Fourier infrared spectrometer. The Zeiss LSM 700 confocal microscope (Zurich, Switzerland) was used to capture the fluorescence and confocal microscopy (CLSM) images. The water contact angle measurement used a Ramé-Hart 200-F1 standard goniometer by the sessile drop method at room temperature with deionized water (2 μL) as the medium. The mechanical testing was obtained with an Instron 5869 testing machine with a tensile speed of 20 mm min^{-1} at room temperature.

S1.3 Material Synthesis.

PCN-222. Synthesis of PCN-222 was performed using the one-pot solvothermal method. Briefly, Zirconyl chloride octahydrate (37.5 mg), TCPP (6.5 mg), and DA (0.3 mL) were mixed in a Pyrexse vial with 16 mL DMF. After ultrasonication for 15 min, the mixture was heated in a 130 ℃ oven for 18 h. The cubic dark purple product was centrifuged and washed several times using DMF and EtOH. The resultant NMOFs was finally dried in an oven for 24 h at 70 ℃ to clear away the poisonous organic solvent.

PCN-Mo-35/80. Zirconyl chloride octahydrate (37.5 mg), TCPP (6.5 mg), TMA (35/80 mg), and DA (0.2 mL) were mixed in a Pyrexse vial with 16 mL DMF. After ultrasonication for 15 min, the mixture was heated in a 130 ℃ oven for 24 h. The greyish green product was centrifuged and washed several times using DMF and EtOH. The resultants NMOFs were finally dried in an oven for 24 h at 70 ℃ to clear away the poisonous organic solvent.

NPCN-Mo. NPCN-Mo was prepared using the same method as that described in PCN-Mo -80 except that DA (0.2 mL) was replaced with DA (0.05 mL).

PLA-PEG-PLA. Triblock copolymer PLA–PEG–PLA was prepared by the ring-opening polymerization of LA with PEG as a macroinitiator and $Sn(Oct)_2$ as a catalyst in a toluene solution.

Preparation of MMMs.

In a typical strategy for the preparation of MMMs, 5 mg of NPCN-Mo was dispersed in 400 μL DCM, 12 mg of PLA was dissolved in 120 μL DCM, and 8 mg of PEG-PLA was dissolved in 40 μL DCM, respectively. The solutions mentioned above were sonicated separately for 45 minutes, then they were mixed together and continued to be sonicated for 30 minutes. The obtained casting solution was slowly casted onto a round coverslip, and then placed on the plane heater at 37 ℃ overnight to evaporate solvent. The resulted PEG-MMMs were further dried by a nitrogen flow at 37 ℃ for 3 h. Pure PLA membranes and PLA-MMMs were prepared in a similar way as described above.

S1.4 Photothermal activity.

NPCN-Mo nanoparticles aqueous solution at different concentrations (0, 0.3, 0.6, 0.9, 1.2 mg mL^{-1}) and control groups (PCN-222, PMA, and PCN-222+PMA) were irradiated with a continuous-wave NIR laser (808 nm, 1 W cm^{-2}) for 600 s to determine the photothermal properties. Different laser intensity (0.5, 0.75, 1, 1.4, 1.6 W cm^{-2}) were also used to verify the favorable photothermal effects of NPCN-Mo (0.9 mg mL^{-1}). The mixture solution of NPCN-Mo (0.9 mg mL^{-1}) in the presence of DTT at different values (0, 1, 10, 50 mM) was exposed to an 808 nm of 1 W cm^{-2} laser for desired times (600 s). The temperature changes of the solution in the entire process were recorded using a thermocouple feeler every 10 s.

S1.5 Photothermal conversion efficiency.

Photothermal conversion efficiency (PCE) of the as-synthesized NPCN-Mo was calculated according to the previous method. Firstly, the NPCN-Mo solution (0.9 mg mL^{-1}) was irradiated with a laser (808 nm, 1 W cm^{-2}) for 10 min and then the laser resource equipment was turned off. After about 10 min, the temperature of the solution dropped to near room temperature. The photothermal conversion efficiency (η) was calculated according to the equation (Eq): $\eta = \frac{hA\Delta T_{max} - Q_S}{I(1-10^{A\lambda})}$, where $\boldsymbol{h}$ is the heat transfer coefficient, $\boldsymbol{A}$ is the surface area of the container, $\boldsymbol{\Delta T_{max}}$ is the maximum temperature change, $\boldsymbol{I}$ is the laser power, $\boldsymbol{A_\lambda}$ is the absorbance at 808 nm, $\boldsymbol{Q_s}$ is the heat associated with the light absorbance of the solvent.

S1.6 Singlet oxygen generation measurements.

The mixture solution of NPCN-Mo (100 μg mL^{-1}) in presence of DCFH-DA (0.005 mM) was dispersed in deionized water and irradiated with an 808 nm laser (1 W cm^{-2}) for 10 min. The whole process was monitored by the FLS980 fluorescence spectrometer every 5 min. The characteristic absorption of 529 nm can be observed on the FL spectrum to verify the generation of the ROS reaction.

S1.7 Bacterial assays

The antibacterial activity of the NPCN-Mo nanoparticles was investigated against *Escherichia coli* (*E. coli*) and *staphylococcus aureus* (*S. aureus*). Both *S. aureus* and *E. coli* were cultured in lysogeny broth (LB) medium at 37 ℃ overnight and harvested during the mid-log phase via centrifugation. The cell pellet was suspended in fresh medium and diluted to 1×10^9 CFU mL^{-1} before use. Then, the bacterial suspension with defined concentration was incubated with the samples for 0.5 h at 37 ℃ in a 96-plate well.

Broth dilution assay: For the broth culture growth-inhibition assays, the bacterial suspensions were exposed to an 808nm laser of 1 W cm^{-2} for 10 min and diluted by PBS to an A630 value of 0.045 (10^3 CFU mL^{-1}). Afterward, 0.2 mL of the diluted bacterial solution was placed into the 96-plate well and cultured for 18 h at 37 ℃. UV-vis absorption at 630 nm was used to measure the optical density of bacteria to prove the antibacterial ability of the different materials.

Colony counting assay: After different treatments against *E. coli* and *S. aureus*, the bacterial suspensions were serially diluted in PBS solution to 10^4 CFU mL^{-1}. A 100 μL portion of the diluted bacterial suspension was placed on gelatinous LB agar plates and incubated at 37 ℃ for 18 h. The percentage of viable cells was then determined by counting the colony-forming units.

Scanning electron microscopy: The morphological changes of bacteria after various treatments were studied by scanning electron microscopy. After killing bacteria experiment, the samples were then fixed in 4% paraformaldehyde solution for 1 h at room temperature. Samples were dehydrated in a series of ethanol solutions (30, 50, 70, 85, 95, 100%), and air-dried for 12 h.

Live/Dead staining assay: A standard live/dead staining assay was performed to observe the formed biofilm intuitively. 500 μL bacterial suspensions at a concentration of 10^7 CFU mL^{-1} were added into the 24-plate well and incubated at 37 ℃ for 24 h. The surface is then gently rinsed with PBS to remove planktonic bacteria. After incubation with NPCN-Mo nanoparticle solution and NIR irradiation as described above, the cultured biofilms were incubated in an oven for another 4 h. Then, 150 μL of staining solution (3.6% SYTO-9 and 3.3% PI) was dropped on the surface and kept in dark for 20 min. Aspirate the staining solution from the well, and the formed biofilm were observed using confocal laser scanning microscopy at 20x objective.

S1.8 Photothermal properties of MMMs.

To evaluate the photothermal properties of the as-prepared PEG-MMMs, 0.5 cm×0.5 cm membrane was immersed in a 96-plate well containing 200 μL aqueous solution, and exposed to NIR laser for 10 min at the power density of 1 W cm^{-2}. And five laser on/off cycles were used to verify the photothermal stability of membrane while 10 wt% PEG-MMMs was used as the experimental group. The thermocouple probe was used to measure the temperature change of the aqueous solution during the whole process, and the data was stored every 10 s in the SD card.

To determine the photothermal properties of the PEG-MMMs surface, the completely dried samples were continuously irradiated with an 808 nm laser for 1 min, and temperature data were recorded using an infrared thermal imaging camera.

S1.9 *In vitro* bactericidal activity of MMMs.

Live/Dead staining assay: The membrane was immersed in 75% ethanol solution for 10 min, and then washed three times with PBS. The sample in a 24-well plate containing *S.aureus* suspension of 10^7 CFU mL^{-1} was incubated at 37 ℃ for 4 h, and treated with/without the NIR light irradiation (1 W cm^{-2}) for 10 min. Then, the attached bacteria were stained with the mixed solution of SYTO 9 and PI for 20 min in dark. Images were obtained under a fluorescent confocal microscope to observe live cells in green and dead cells in red.

Scanning electron microscopy: The morphologies of the attached *S.aureus* on the membrane surface with/without NIR laser irradiation were observed by SEM. After killing bacteria experiment, transfer the membrane to a 24-well plate containing 1 mL

of culture medium and incubate in an oven at 37 ℃ for 48 h. After washing the membrane surface with PBS, bacterial cells were fixed with paraformaldehyde (4%) for 3 h at room temperature. Afterward, the dehydration was preceded using increasing concentrations of ethanol (30%, 50%, 70%, 85%, 95%, and 100%) for 15 min, and air-dried.

Cyclic Antibacterial Test: Briefly, the membrane was immersed in a suspension of *S.aureus/E.coli* bacteria (200 μL, 10^9 CFU mL^{-1}) and irradiated with/without an 808 nm NIR laser for 10 min. For the measure of bacterial viability, suspensions were serial dilutions (10^4 CFU mL^{-1}) plated on LB agar plates in triplicate. Colonies were counted on the plates after 18 h growth at 37 ℃.

S1.10 Dye Absorption of MMMs.

The prepared PEG-MMMs were immersed in 2 mL of 0.05 mM methylene blue aqueous solution for 24 h at room temperature. The pure PLA membrane was also tested for dye absorption under the same conditions for comparison.

Section S2. Supplementary results

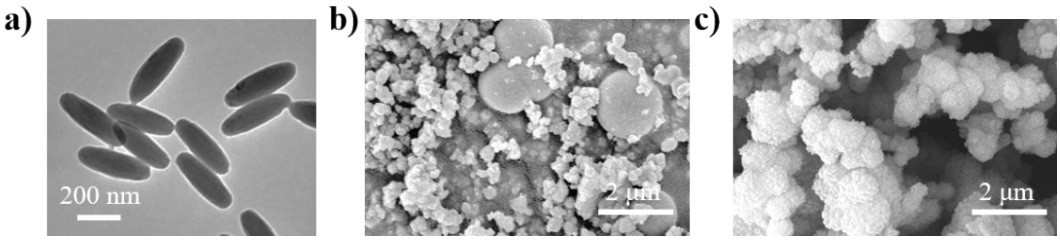

Figure S1. (a) TEM image of PCN-222. Scale bars: 200 nm. SEM images of (b) PCN-Mo-35 and (c) PCN-Mo-80. Scale bars: 2 μm.

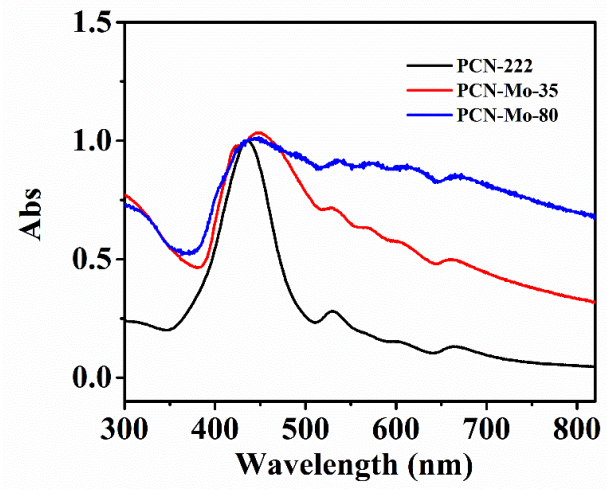

Figure S2. UV-vis absorption spectra of PCN-222, PCN-Mo-35 and PCN-Mo-80 in DMF solution.

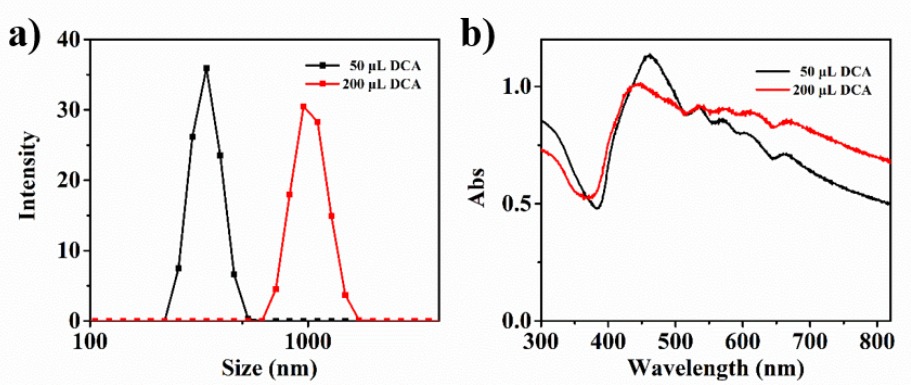

Figure S3. (a) Size distribution of PCN-Mo with different contents of DCA in aqueous solution. (b) UV-vis absorption spectra of PCN-Mo with various contents of DCA in DMF solution.

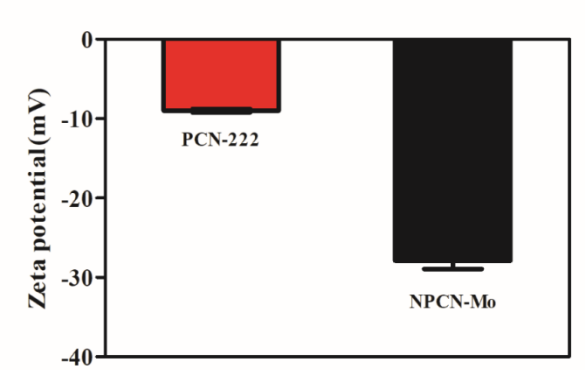

Figure S4. The zeta potential of PCN-222 and NPCN-Mo.

Table S1. Fluorescence quantum yield of PCN-222 and NPCN-Mo NMOFs in DMF.

Sample	PCN-222	NPCN-Mo
Yf (%)	0.023	0.003

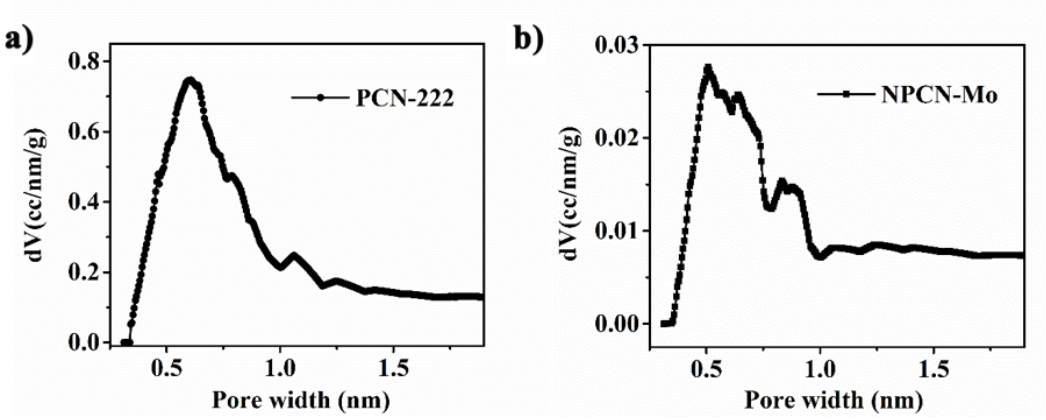

Figure S5. Pore size distributions of PCN-222 and NPCN-Mo.

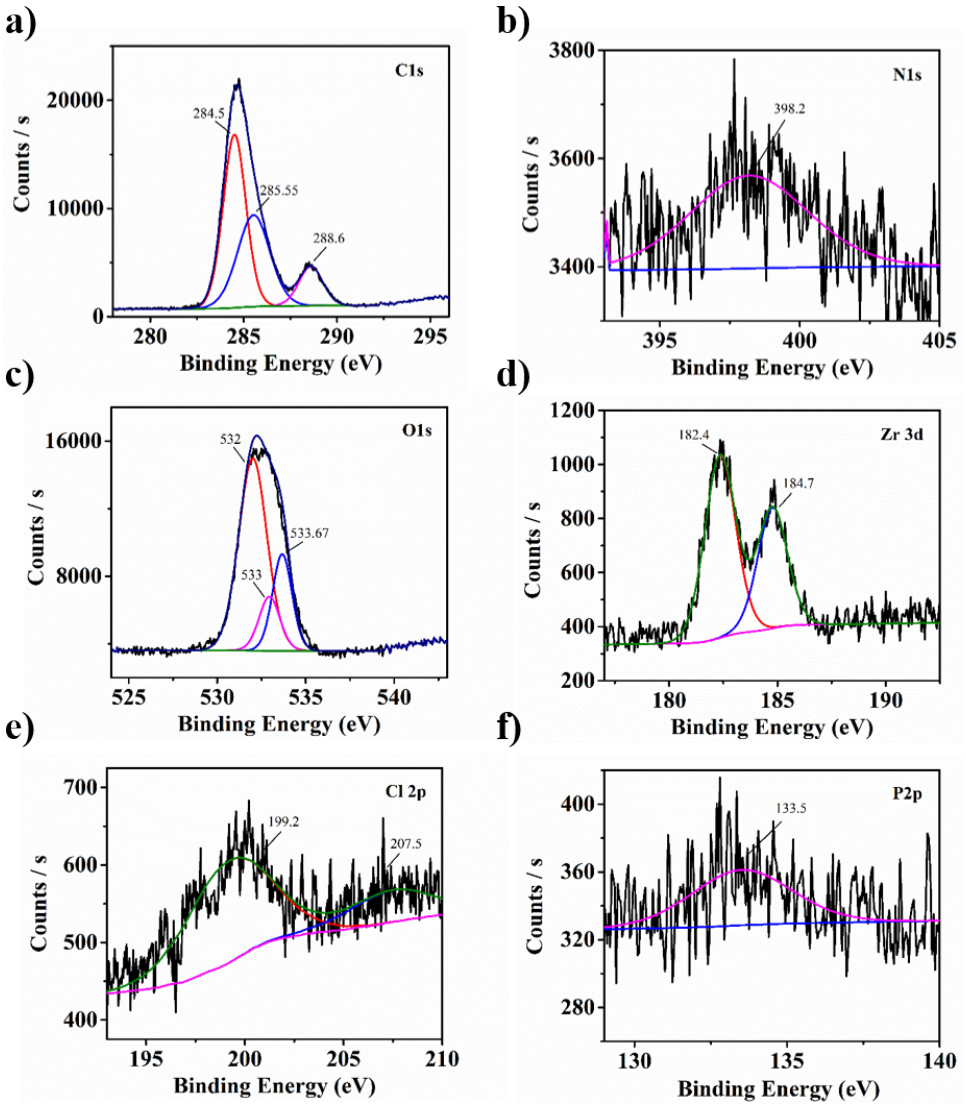

Figure S6. X-ray photoelectron spectroscopy spectra of (a) C 1s, (b) N 1s, (c) O 1s, (d) Zr 3d, (e) Cl 2p, and (f) P 2p of NPCN-Mo.

Table S2. Inductively Coupled Plasma Mass Spectrometry (ICP-MS) Analysis of NPCN-Mo.

Mo	Zr
166.5 ppm	177.7 ppm

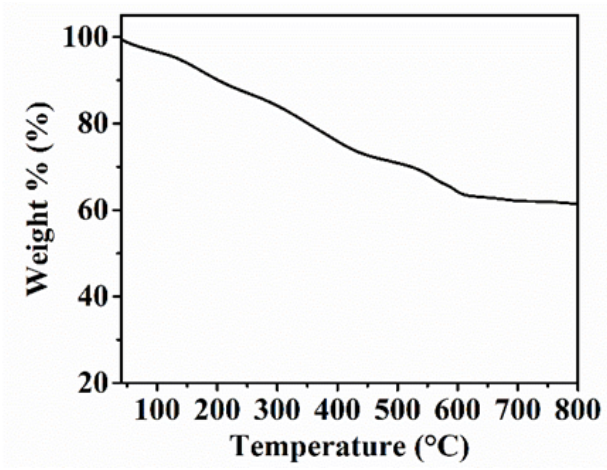

Figure S7. Thermal gravimetric analysis (TGA) of NPCN-Mo from 40 to 800 °C at rate of 10 °C min^{-1}.

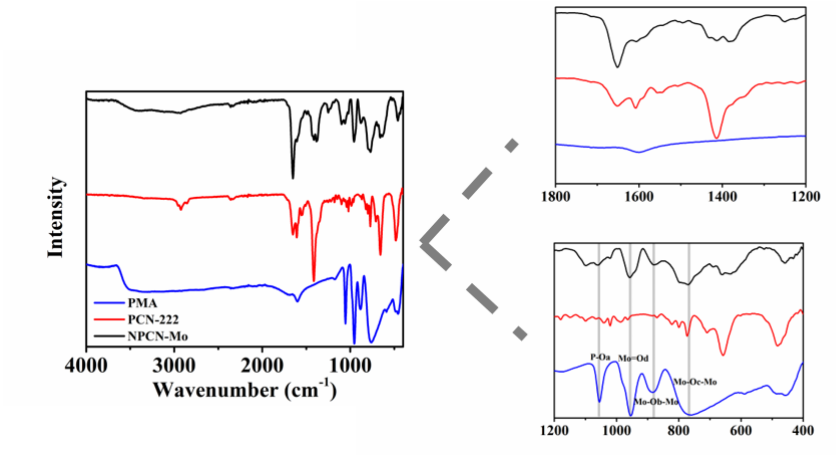

Figure S8. FT-IR spectra of NPCN-Mo. The FT-IR spectra of as-synthetic nano-particles have four absorption bands at 1055, 958, 866, and 786 cm^{-1}, corresponding to P-O_a (a: tetrahedral oxygen atom), Mo-O_d (d: terminal Oxygen), Mo-O_b-Mo (d: bridging oxygen) and Mo-O_c-Mo (c: edge-shared oxygen atoms) vibrations. The vibrational bands of PCN-222 between 1300 and 1750 cm^{-1} were clearly observed in the IR spectrum of NPCN-Mo, which is attributed to the carboxylate vibration of the organic linkers.

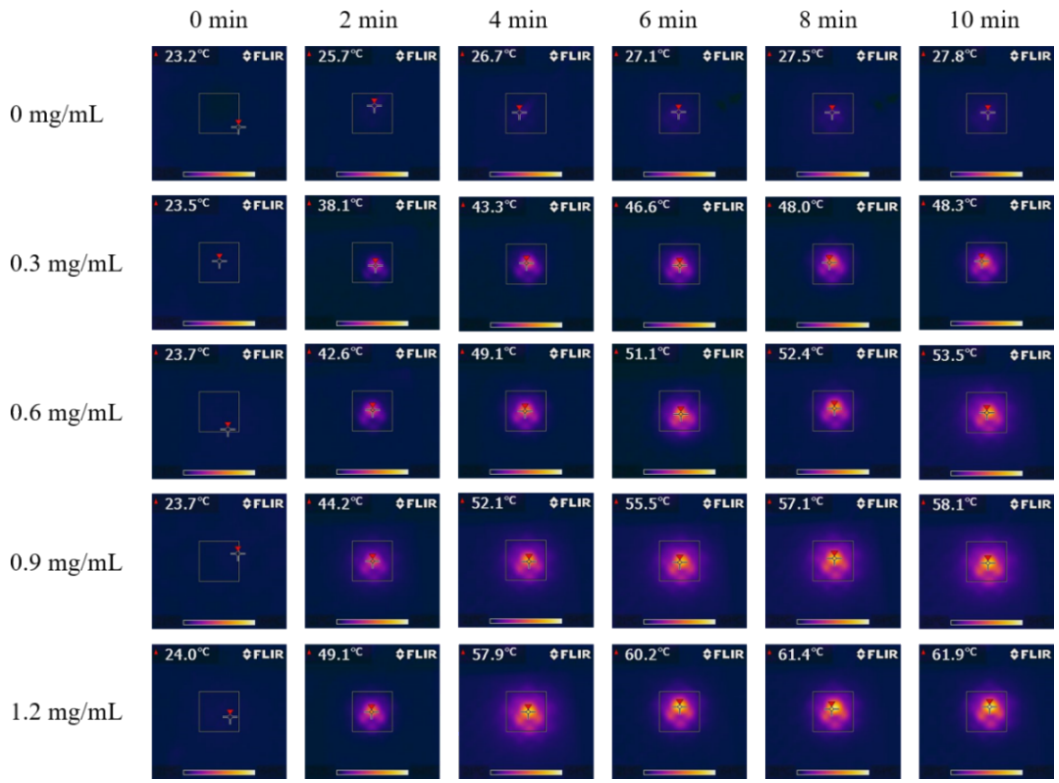

Figure S9. The photothermal images of various concentrations NPCN-Mo under 10 min of laser illumination (808 nm, 1 W cm^{-2}, V = 200 μL) at the 2 min interval.

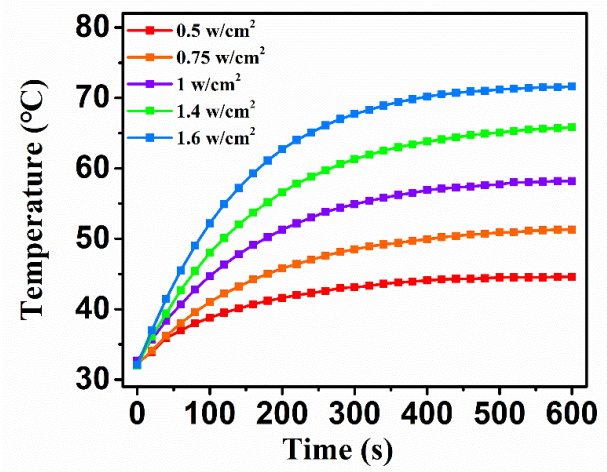

Figure S10. Temperature heating curves of NPCN-Mo aqueous solutions with the same concentration of 0.9 mg mL^{-1} under different laser powers (0.5, 0.75, 1, 1.4, and 1.6 W cm^{-2}) after 10 min NIR irradiation.

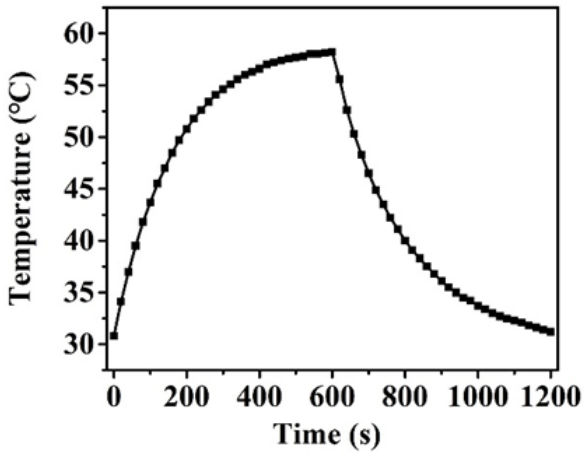

Figure S11. Photothermal effect of the NPCN-Mo solution (0.9 mg mL^{-1}) under laser irradiation, which was turned off after 10 min of irradiation.

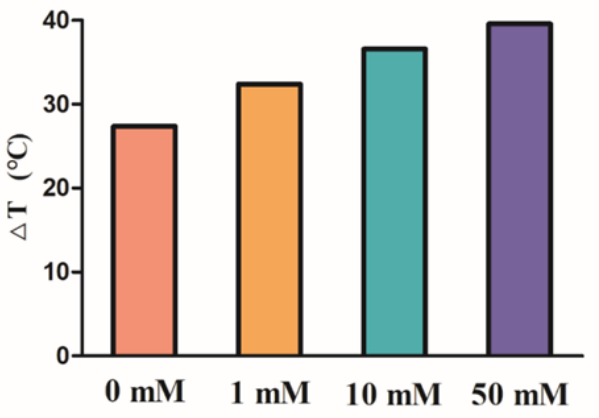

Figure S12. The temperature variation of NPCN-Mo (0.9 mg mL^{-1}) in the presence of DTT with different concentrations (0, 1, 10, 50 mM) under NIR irradiation at a power density of 1 W cm^{-2} for 10 min.

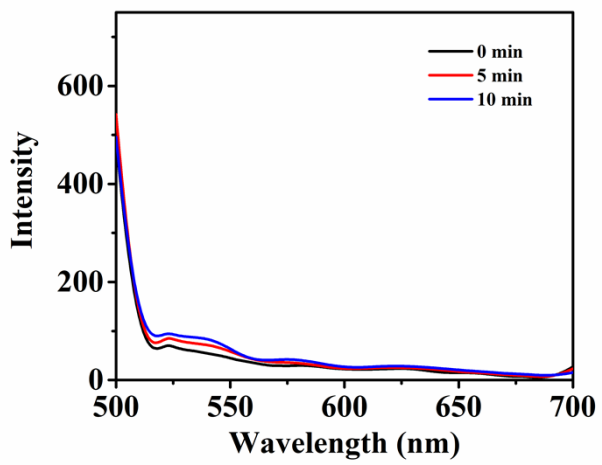

Figure S13. The FL spectrum of the solution of NPCN-Mo (100 μg mL^{-1}) in the presence of DCFH-DA under 808 nm laser (1 W cm^{-2}) irradiation for 10 min.

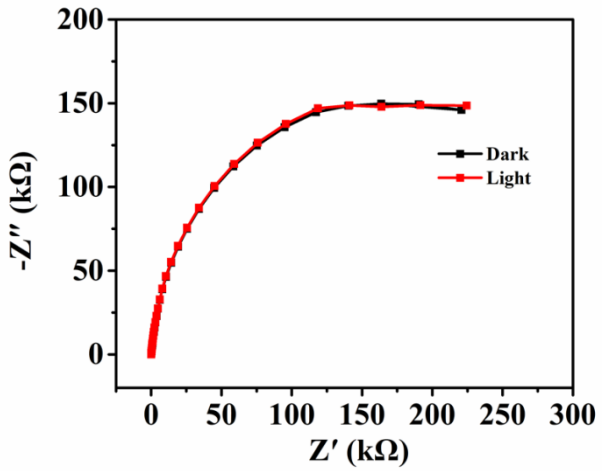

Figure S14. EIS Nyquist plots of PCN-222 in the dark and NIR light states.

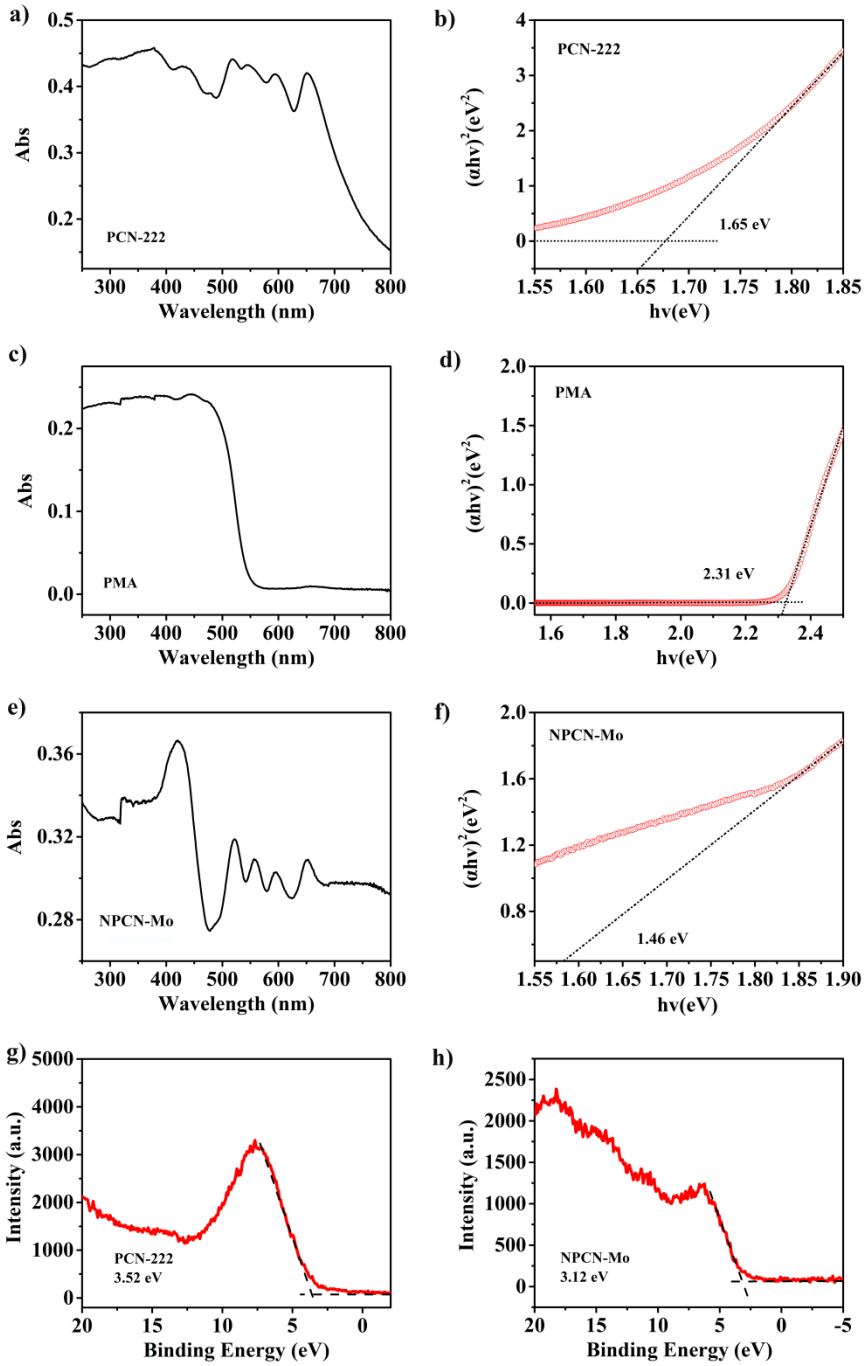

Figure S15. (a-b) UV-vis reflectance spectrum of PCN-222 and its band gap estimated from UV-vis reflectance spectrum. (c-d) UV-vis reflectance spectrum and band gap of PMA. (e-f) UV-vis reflectance spectrum and band gap of NPCN-Mo. (g-h) Valence band (VB) XPS spectra of PCN-222 and NPCN-Mo.

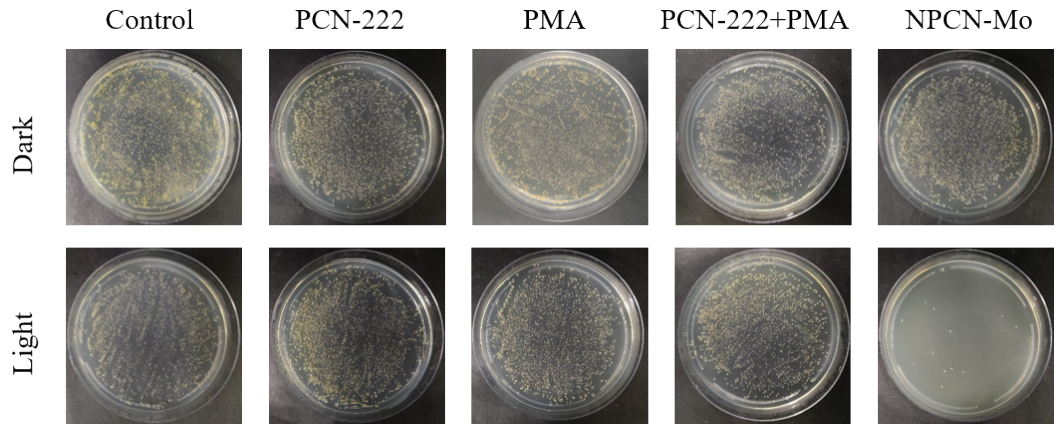

Figure S16. Typical photographs of *S. aureus* colonies formed on agar plates for different treatments (PBS, PCN-222, PMA, PCN-222+PMA, NPCN-Mo) with/without NIR irradiation. The NIR irradiation condition is 1 W cm^{-2} for 10 min.

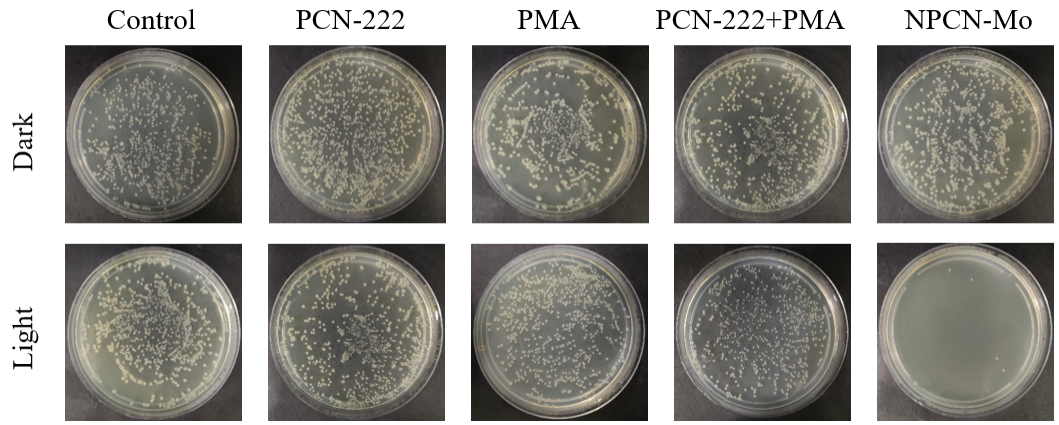

Figure S17. Typical photographs of *E. coli* colonies formed on agar plates for different treatments (PBS, PCN-222, PMA, PCN-222+PMA, NPCN-Mo) with/without NIR irradiation. The NIR irradiation condition is 1 W cm^{-2} for 10 min.

Table S3. Selected photoactive antibacterial materials in comparison with as-synthesized NPCN-Mo in this work.[2-12]

Samples	Key Component	Wavelength and Intensity	Initial bacterial concentration (CFU mL ^{1})	Type of bacteria and Sterilization efficiency	Ref.
NPCN-Mo	Porphyrin, Mo-MOF (Photothermal)	808 nm (1 W cm^{-2})	10^9	E. coli (99%, 0.9 mg mL^{-1}, 10 min) S. Aureus (99%, 0.9 mg mL^{-1}, 10 min	This work
4-PtTPyPor	Pt, porphyrin (Photodynamic)	Red light (50 mW cm^{-2})	10^5	E. coli (99.9%, 1362 μg mL^{-1}, 60 min) S. Aureus (99.9%, 681 μg mL^{-1}, 60 min)	S1
BDP-C60	BDP, C60 (Photodynamic)	Green light (5 mW cm^{-2})	10^8	E. coli (99.99%, 1 μM, 30 min) S. Aureus (99.99%, 1 μM, 15 min)	S2
Ag/TiO_2 film	Ag, TiO_2 (Photocatalysis)	UVC light (20 μW cm^{-2})	10^6	E. coli (99.9%, 0.2 mg cm^{-2}, 60 min)	S3
ZIF-8	Zn-MOF (Photodynamic)	A 300 W Xe lamp (100 mW cm^{-2})	10^7	E. coli (99.9999%, 0.5 mg mL^{-1}, 120min)	S4
Ag_9-AgTPyP	Porphyrin, Ag (Photodynamic)	White LED lamp (80 mW cm^{-2})	10^8	MRSA (99.999%, 0.05 mg mL^{-1}, 120 min) P.aeruginosa (99.99999%, 0.05 mg mL^{-1}, 90 min)	S5
MoS_2-modified fabrics	MoS_2 (Photothermal)	a solar simulator (1 W m^{-2})	10^6	E. coli (100%, MoS_2 nanosheet suspension 500μg mL^{-1}, 5 min) S. Aureus (100%, MoS_2 nanosheet suspension 500μg mL^{-1}, 5 min)	S6
UTG-PVDF	UCNPs@TiO_2, GO (Photodynamic and Photothermal)	980 nm (2.5 W cm^{-2})	10^7	E. coli (>95%, 10 wt %, 5 min) S. Aureus (>95%, 10 wt %, 5 min)	S7
MoS_2-CeO_2	MoS_2, CeO_2 (Photothermal)	808 nm (1 W cm^{-2})	10^7	E. coli (99%, 0.1 mg mL^{-1}, 5 min) S. Aureus (99%, 0.1 mg mL^{-1}, 5 min)	S8
ZnO-CNP-TRGL	Nanocarbon MOF with Zn^{2+} (Photothermal)	808 nm (2 W cm^{-2})	10^6	E. coli (100%, 0.05 mg mL^{-1}, 5 min) S. Aureus (100%, 0.05 mg mL^{-1}, 5 min)	S9
CF@PCN	PCN-224, Ti_3C_2 (Photothermal and Photodynamic)	a Xe lamp (500 W, 15 cm sample distance, λ ≥ 420 nm)	10^8	E. coli (99.9999%, 30 min) S. Aureus (99.9999%, 30 min)	S10
PMCS@MNs	ZIF-8 derivatives with Zn^{2+} (Photothermal)	808 nm (1 W cm^{-2})	10^8	S. Aureus (99.13%, 5 min)	S11

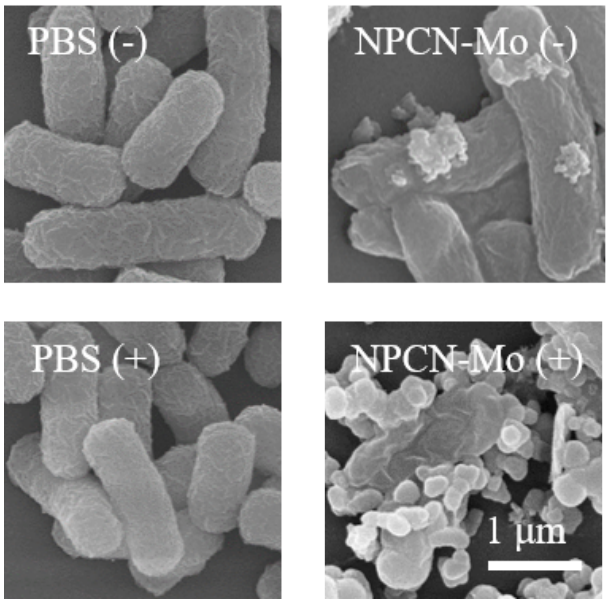

Figure S18. SEM images of *E. coli* treated with PBS and NPCN-Mo under various conditions.

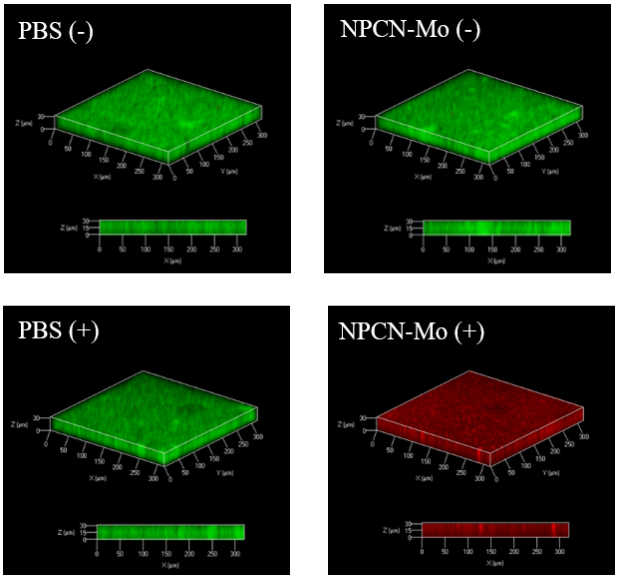

Figure S19. CLSM images of the *E.coli* biofilms treated with PBS and NPCN-Mo with/without NIR irradiation. The bacteria were stained by SYTO 9 (green) and PI (red). The NIR irradiation condition is 1 W cm^{-2} for 10 min.

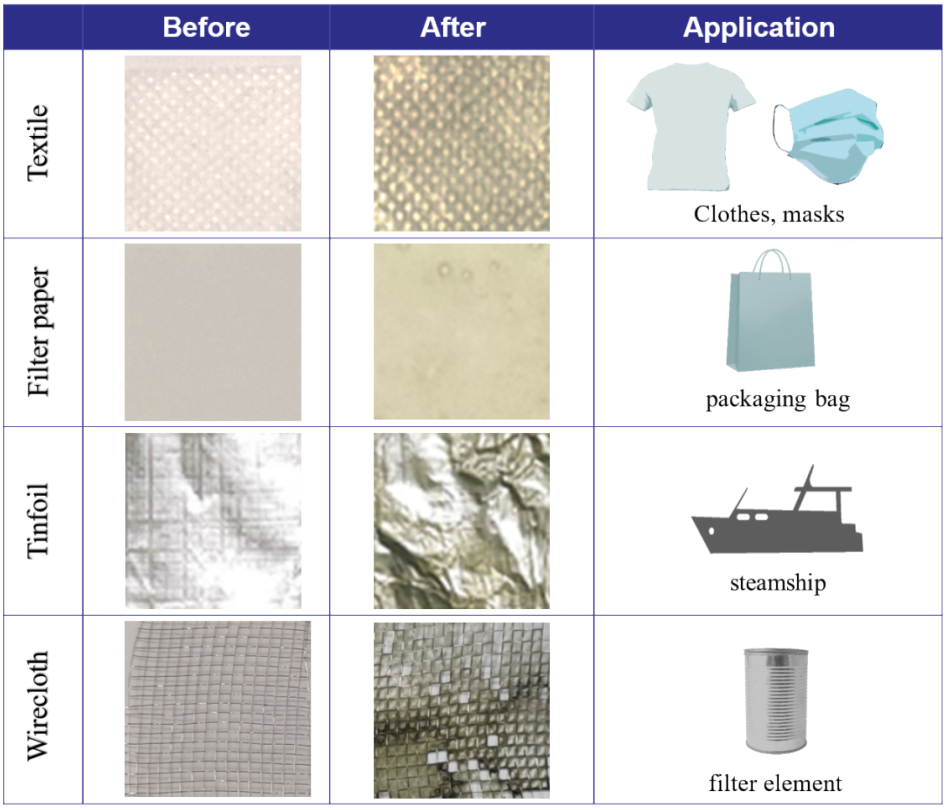

Figure S20. Representative photographs of material surfaces (non-woven fabric 2.4 cm × 2.4 cm, filter paper 2.4 cm × 2.4 cm, tinfoil 2.4 cm × 2.4 cm, mesh wire 2.4 cm × 2.4 cm) before and after modification of PEG-MMMs nanocoating at room temperature.

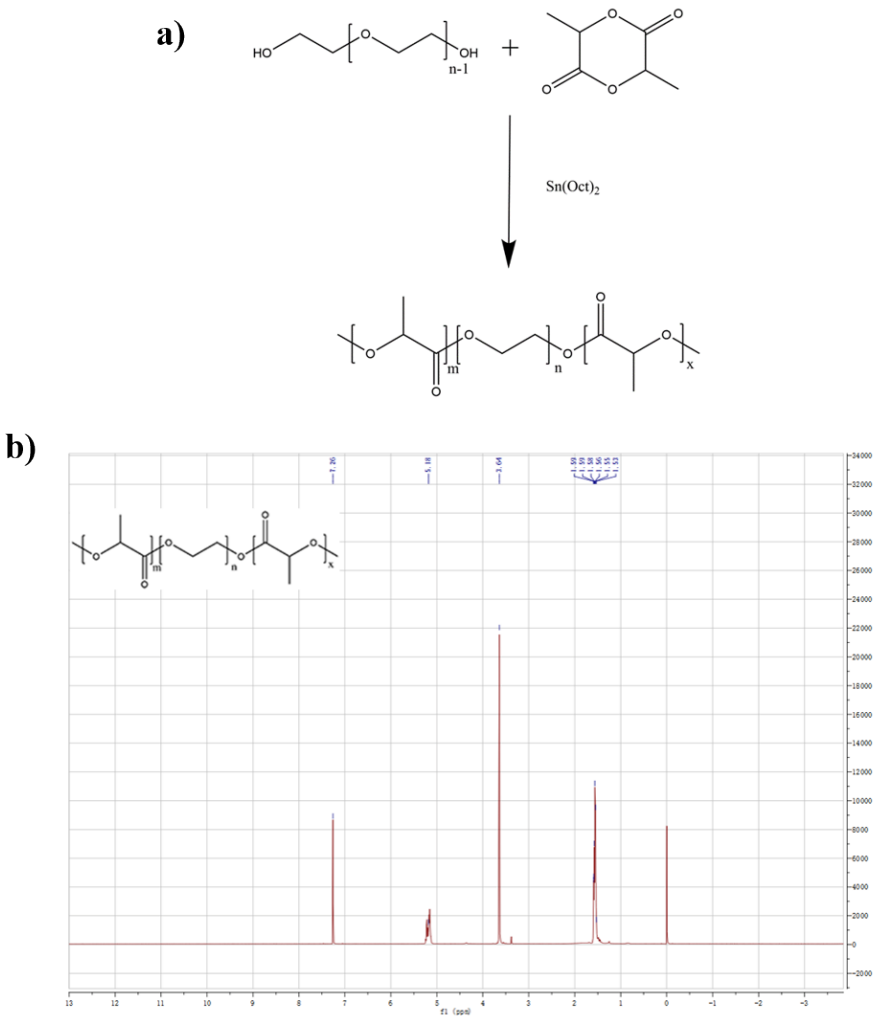

Figure S21. (a) The synthesis process of PLA-PEG-PLA refers to the previous work.[13] (b) ^{1}H NMR spectrum of PLA-PEG-PLA in $CDCl_3$, the obtained triblock copolymer with an average molecular of 8780.

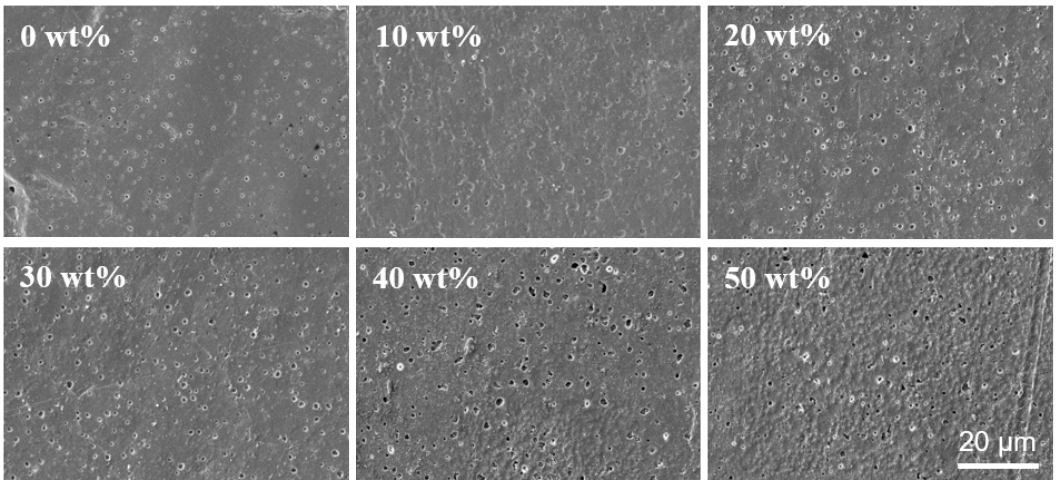

Figure S22. SEM images of as-synthesized PEG-MMMs under the top view. Scale bars: 20 μm.

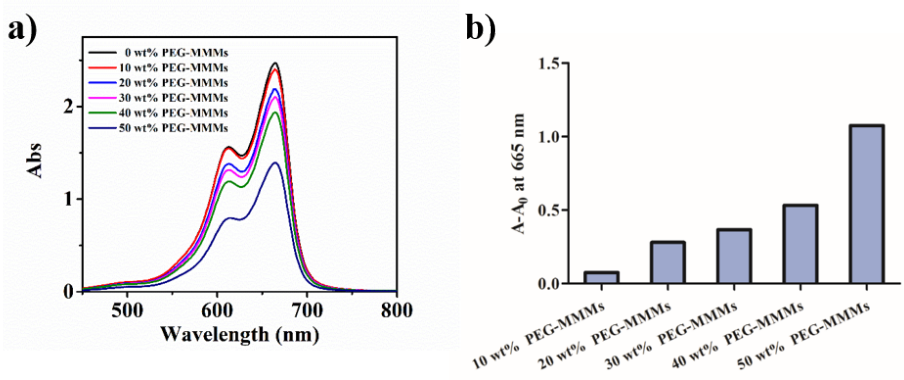

Figure S23. Adsorption performance of the PEG-MMMs towards 0.05 mM methylene blue. (a) UV-vis absorption spectra of the MB solution after soaking PEG-MMMs into the solution for 24 h. (b) The corresponding amount of decrease in UV-vis absorption intensity of the MB solution.

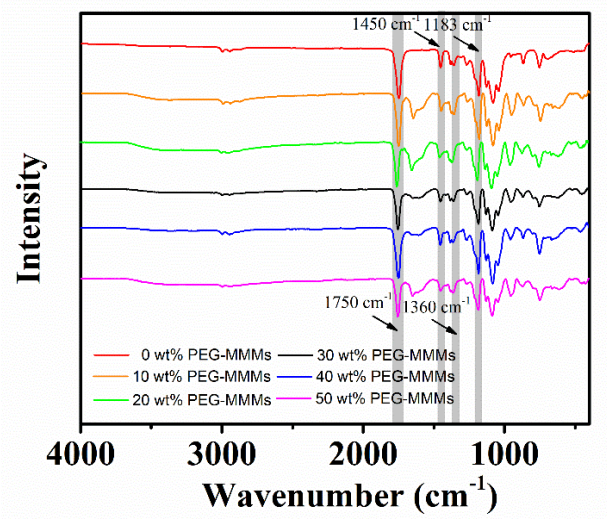

Figure S24. Fourier transform infrared (FT-IR) spectra of PEG-MMMs with various NPCN-Mo contents.

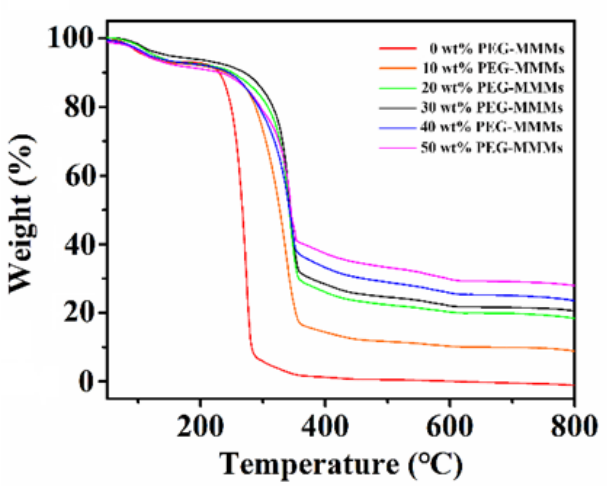

Figure S25. TGA curves of PEG-MMMs with various NPCN-Mo contents.

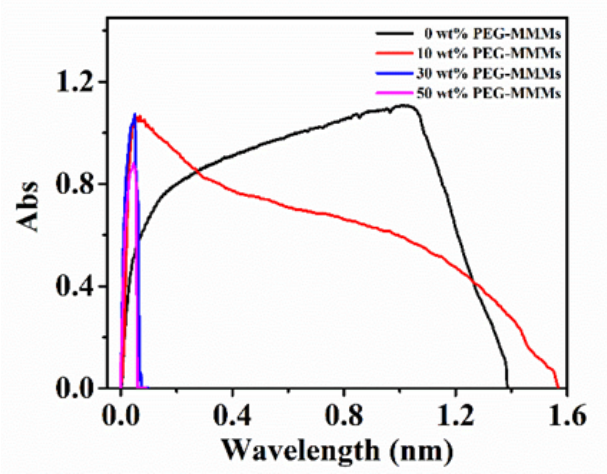

Figure S26. The stress-strain curves of PEG-MMMs with different NPCN-Mo contents.

Table S3. Results of the Elastic Modulus, Ultimate tensile strength, and elongation at break for PLA and PEG-MMMs with different NPCN-Mo contents.

Sample	Elastic Modulus (MPa)	Ultimate tensile strength (MPa)	Elongation at break (%)
PLA	182	11.1	180
10 wt% PEG-MMMs	513	10.7	160
30 wt% PEG-MMMs	793	10.7	4.6
50 wt% PEG-MMMs	436	8.83	6.1

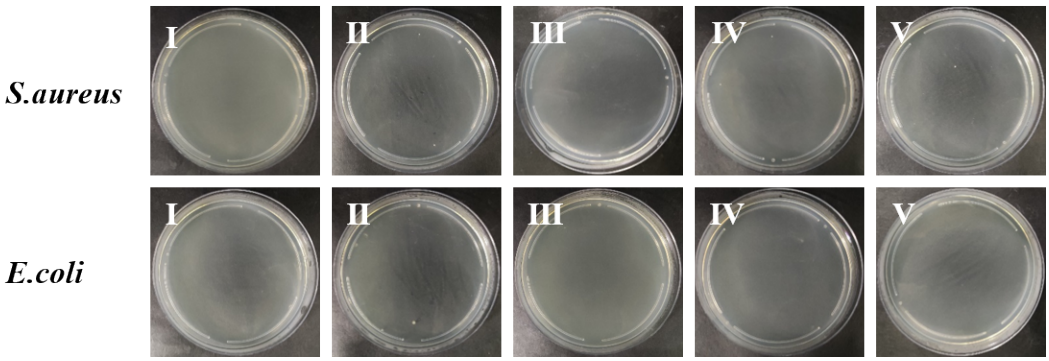

Figure S27. Typical photographs of bacterial colonies formed on agar plates for recycling bactericidal performance test of 10 wt% PEG-MMMs with NIR irradiation.

Reference

[1] S. Yuan, J.-S. Qin, L. Zou, Y.-P. Chen, X. Wang, Q. Zhang and H.-C. Zhou, J. Am. Chem. Soc., **2016**, *138*, 6636-6642.

[2] L. Q. Soares Lopes, A. P. Ramos, P. M. Copetti, T. V. Acunha, B. A. Iglesias, R. C. Vianna Santos, A. K. Machado, M. R. Sagrillo, Microb. Pathog., **2019**, *128*, 47.

[3] M. L. Agazzi, J. E. Durantini, N. S. Gsponer, A. M. Durantini, S. G. Bertolotti, E. N. Durantini, ChemPhysChem, **2019**, *20*, 1110.

[4] B. Moongraksathum, M. Y. Chien, Y. W. Chen, J. Nanosci. Nanotechnol. Appl., **2019**, *19*, 7356.

[5] P. Li, J. Li, X. Feng, J. Li, Y. Hao, J. Zhang, H. Wang, A. Yin, J. Zhou, X. Ma, B. Wang, Nat. Commun., **2019**, *10*, 2177.

[6] M. Cao, S. Wang, J. H. Hu, B. H. Lu, Q. Y. Wang, S. Q. Zang, Adv. Sci., **2022**, *9*, 2103721.

[7] P. Kumar, S. Roy, A. Sarkar, A. Jaiswal, ACS Appl. Mater. Interfaces, **2021**, *13*, 12912.

[8] J. Sun, L. Song, Y. Fan, L. Tian, S. Luan, S. Niu, L. Ren, W. Ming, J. Zhao, ACS Appl. Mater. Interfaces, **2019**, *11*, 26581.

[9] T. Ma, X. Zhai, Y. Huang, M. Zhang, X. Zhao, Y. Du, C. Yan, Adv. Healthcare Mater., **2021**, *10*, 2100033.

[10] X. Nie, S. Wu, F. Huang, Q. Wang, Q. Wei, ACS Appl. Mater. Interfaces, **2021**, *13*, 2245.

[11] Y. Sun, J. Liu, H. Wang, S. Li, X. Pan, B. Xu, H. Yang, Q. Wu, W. Li, X. Su, Z. Huang, X. Guo, H. Liu, Adv. Funct. Mater., **2021**, *31*, 2100218.

[12] Y. Yang, Y. Deng, J. Huang, X. Fan, C. Cheng, C. Nie, L. Ma, W. Zhao, C. Zhao, Adv. Funct. Mater., **2019**, *29*, 1900143.

[13] Z. Xie, T. Lu, X. Chen, C. Lu, Y. Zheng, X. Jing, J. Appl. Polym. Sci., **2007**, *105*, 2271.